Desalination and Water Treatment
www.deswater.com

doi: 10.5004/dwt.2021.27642

234 (2021) 348–360
September

Newly developed nanofiltration membrane blended with mesoporous silica with low transmembrane pressure and excellent anti-fouling performance

Ying Ding[a,*], Jianzhong Zhu[b], Dong Liu[c]

[a]*College of Environment Science, Nanjing Xiaozhuang University, Nanjing 211171, China, Tel. +86 18751958626; email: xiaozhuangdy@126.com*
[b]*College of Environment, Hohai University, Nanjing 210098, China, Tel. +86 13739186298; email: 987203352@qq.com*
[c]*Suzhou Erye Pharmaceutical Co., Ltd., Suzhou 215152, China, Tel. +86 15921277065; email: 569399078@qq.com*

Received 12 December 2020; Accepted 25 July 2021

ABSTRACT

The membrane separation process has disadvantages of high transmembrane pressure and fouling. In this study, the blend membranes were prepared using the phase inversion method, which was added different contents (from 0 to 1.0 wt.%) precursor of mesoporous silica (M-Si) in membrane matrix and calcined with high temperature after membrane forming. The existence of M-Si was proved using characterization methods of N_2 adsorption/desorption tests, viscosity analysis, X-ray photoelectron spectroscopy, static contact angle, zeta potential and small-angle X-ray diffraction. Because of the addition of M-Si, the membrane structure and morphology was changed, the supporting layer was eliminated, the pore size was narrowed and the homogeneity was altered, which were shown by scanning electron microscopy (SEM) and molecular weight cutoff. Under the pressure of 0.15 MPa, tests of water flux, salt rejection and antifouling property were used as criteria to characterize the prepared membranes. Results showed that adding M-Si particles in the membrane could decrease the water flux and improve the rejection of $MgSO_4$. Moreover, the water content and anti-fouling experiments revealed that the incorporation of M-Si improved membrane hydrophily and enhanced anti-fouling property, obviously. Thereinto, the membrane with 0.2 wt.% M-Si exhibited the best uniformity, the lowest water flux (10.45 L/m^2 h) and the highest flux recovery ratio (96%). Membranes with this fabrication method show excellent fouling resistance property and can reduce energy consumption, indicating that it has promising application prospects in micro-organic filtration and advanced water treatment.

Keywords: Nanofiltration membrane; Mesoporous silica; Transmembrane pressure; Anti-fouling

1. Introduction

Membrane sieving is an emerging technology in separation, purification and concentration, which separates target object from liquid or gas compound due to the permselectivity. With the advantages of energy conservation, no phase transition and secondary pollution, it is widely used in various fields including chemical, water treatment, medicine synthesis and environment protection [1–4]. Nanofiltration (NF) is a type of separation process between reverse osmosis (RO) and ultrafiltration (UF) [5]. Its characteristics which have smaller pore size to separate small molecules materials than UF and low operating pressure, high permeate flux and high rejection of multivalent ions in comparison to RO [6] make it widely applied in water soften [7,8], wastewater treatment [9,10] and drinking water treatment [11–16], recently. The vast majority of nanofiltration membrane is an asymmetric membrane, which has a dense top layer that served as a sieving effect and a porous sub-layer playing a supporting

* Corresponding author.

role with no function in the separation process. The other major rejection mechanism is Donnan exclusion [17,18], caused by charged groups on the membrane surface, resulting in the separation of different charged ions.

The compound process is the most common method for preparing NF membranes, including interfacial polymerization [17,18] and surface coating [19–21]. The principal principle of these two methods is that an ultrathin selective layer is formed by physical coating or chemical polymerization on the substrate surface. However, these two methods have disadvantages of uncontrollable membrane surface morphology and poor mechanical properties, which affect its screening effect and service life. Blending is another common method for NF preparation [22,23]. The flat membrane is made by using blend solution as casting solution with phase inversion process, and pore size can be controlled by adding blend components and changing different components' compatibility. Recently, components such as calcium stearate [24], styrene-maleic anhydride [25] and graphene oxide [26–28] are added in membranes to form a stigmatic symmetric structure or a dense skin layer, shrinking membrane pore size classed as NF.

Nanofiltration membrane needs high transmembrane pressure (0.2–1.0 MPa) in the separation process, which results in great energy consumption and has an influence on membrane mechanical property and service life. Fouling is one problem restricting membrane application range, which is caused by precipitation of non-polar solutes, hydrophobic particles or possibly the growth of bacteria on the membrane surface, leads to the declination of flux, quality of produced water and service life of the NF membrane [25,27]. To overcome this problem, the prepared nanocomposites were doped into the membrane substrate solution such as titanium oxide (TiO_2) [28,29], zirconium oxide (ZrO_2) [30], aluminum oxide (Al_2O_3) [31,32] and silicon dioxide (SiO_2) [33,34] or organic additives like poly(ethylene glycol) methyl ether methacrylate (POEM) [35] to enhance fouling resistance ability by improving membrane surface hydrophilicity [25]. Mesoporous silica materials, the pore size of which is 2–50 nm [36], are synthesized by using hybrid organic-inorganic composites through supramolecular assembly or cooperative effect. With the structures and properties of continuous adjustable, large specific surface area, easily modified mesoporous surface, thermal stability and so on [37–39], mesoporous silica materials were broadly applied in the fields of catalysis, adsorption and separation [40,41].

In this paper, different content of highly ordered mesoporous silica which was prepared by template synthesis method is doped into membranes by phase inversion method [42]. Characterization of transmission electron microscopy (TEM), small-angle X-ray diffraction (SXRD), N_2 adsorption–desorption isotherms, viscosity analysis and X-ray photoelectron spectroscopy (XPS) were used to confirm that the surface structure of the film was improved and the inorganic silicon materials prepared by this method was orderly and mesoporous. The morphology of the blend membranes was characterized by scanning electron microscopy (SEM), zeta potential and static contact angle test (SCA). The effects of modified mesoporous silica on the membrane's performances (water flux, salt rejection, molecular weight cutoff, and anti-fouling performance) were discussed.

2. Materials and methods

2.1. Materials

Polyethersulfone (PES) polymer (Veradel® 3000P), generally used as the main membrane material in the USA, with a specific gravity of 1.37 g/cm^3 purchased from Solvay Specialty Polymers. Anhydrous lithium chloride and polyvinylpyrrolidone (PVP, Mw: 40 kg/mol) were used as pore former agents and N,N-dimethylacetamide as solvent. Triblock copolymer, PEG-PPG-PEG (Pluronic P123), was obtained from Sigma-Aldrich. Polyethylene glycol (400, 600, 1,000, and 2,000), were purchased from Nanjing Chemical Reagent Co., Ltd., (Nanjing, China). Nitrate, ammonia chloride, anhydrous lithium chloride, HCl, ethanol, bovine serum albumin (BSA), tetraethyl orthosilicate (TEOS) were from Nanjing the preferred Chemical Co., Ltd., (Nanjing, China). All these reagents and solvents were of analytical grade and used as received.

2.2. Preparation of the blend membranes

Asymmetric blended membranes were prepared by mingling with mesoporous silica (M-Si) following phase inversion. Firstly, the PES sol was prepared by adding 10 g PES to N,N-dimethylacetamide (DMAc) and incorporating 1 wt.% anhydrous lithium chloride and 9% (wt.%) polyvinylpyrrolidone (PVP) and stirring 20 h [43]. Secondly, inorganic additive materials were fabricated as follows: 4g P123 was added to a blend aqueous solution of 120 g hydrochloric acid solution (2 mol/L) and 30 g deionized (DI) water. This solution was vigorously stirred for 2 h at 38°C to ensure the complete dissolving of P123. Then, 8.4 g tetraethyl orthosilicate (TEOS) was added to the solution and stirred for about 20 h. The white suspension was placed in a high-pressure batch autoclave at 100°C for 24 h. After that, the precipitate after filtration with the filter paper was rinsed with the mixed solution of DI water and ethanol and dried thoroughly in the oven [24]. Thirdly, the process was followed by the addition of inorganic materials of various loading (0, 0.1, 0.2, 0.5, and 1.0 wt.%) to the sol solution in the first part, stirring for 6 h and standing 72 h. The homogeneous dope solution was cast onto a glass plate by a casting knife with a thickness of 250 μm. After the solvent evaporation for about 2 min, the glass plate was immediately immersed in a coagulation bath containing 15 v% N,N-dimethylacetamide to have an exchange between the solvent (DMAc) and the non-solvent (water). Afterward, the blend membranes were kept in DI water for 24 h [25]. Finally, putting all membranes into the tube furnace for thermal treatment at 120°C for 2 h under the protection of nitrogen atmosphere, and the composite membranes mingled with M-Si were obtained. The schematic outline of the sample preparation is illustrated in Fig. 1.

2.3. Characterization of mesoporous silica (M-Si) and membranes

As the complex composition and multitudinous chemical bands in the membrane, it is difficult to judge the

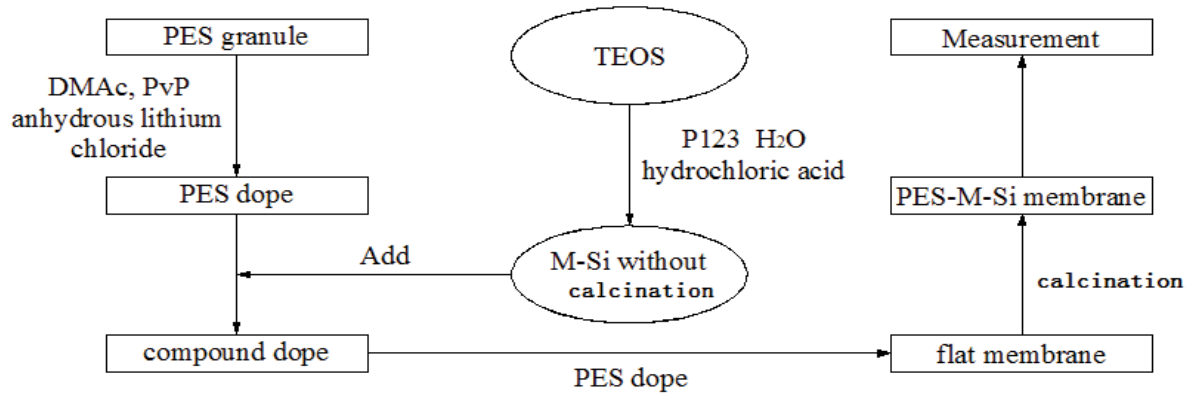

Fig. 1. A synthetic method for PES M-Si composite membranes.

existence of M-Si in many peaks during the analysis of IR spectra [44]. So we calcined M-Si without removing the template at 120°C for 2 h and used characterization methods (the N_2 adsorption/desorption tests and SXRD) to investigate the synthesis of M-Si. Adsorption/desorption experiments of inorganic M-Si using nitrogen as adsorbent were carried out at 77 k on a NOVA 2000e. The specific surface areas were calculated from the adsorption branch using the Brunauer–Emmett–Teller (BET) equation. The pore sizes were calculated from the desorption branch of the isotherm using the Barrett–Joyner–Halenda (BJH) model. XRD patterns of the M-Si were recorded on a Bruker D8 ADVANCE diffractometer with Cu K_α radiation (λ = 0.154 nm) in the 2θ ranges of 0.6°–10° (SXRD). In this paper, Thermo ESCALAB 250Xi X-ray photoelectron spectroscopy (XPS) of Thermo ESCALAB 250Xi was used to determine the percentage content of main elements on the surface of the blend film and the energy spectrum was analyzed by XPS PEAK 1.0 software. The hydrophilicity of the blend nanofiltration membrane was tested by the OCA20 automatic contact angle measuring instrument produced by the Data Physics Company of Germany. The contact angle tester uses a 0.5 mm diameter needle to drop 3 μL of water onto the surface of the test film. The zeta potential of the blend film was measured by SurPASS potential analyzer. The experimental process is divided into the following steps: (1) put the test sample into the test cell, separate the two samples with silica gel gasket and place Ag/AgCl reverse electrode on both sides of the membrane; (2) the test solution is 0.001 mol/L KCl electrolyte solution and zeta potential on the membrane surface is measured by Helmholtz–Smoluchowski equation. The morphology of membranes was characterized by SEM. Before SEM observation, the fabricated membranes were frozen in liquid nitrogen and then ruptured. The surface and cross-section of the membranes were sputtered with gold and observed using SEM.

2.4. Water flux and salt rejection

The water flux and salt rejection are important basic parameters of the membrane. The membrane performance was investigated using a lab-permeation test under normal conditions. Before the membrane filtration tests, membranes need to be pre-pressurized with DI water for 5min at 0.15 MPa to reach a steady state. Flux is introduced cased in the following equation [45]:

$$\mathrm{WF} = \frac{V}{A \times t} \tag{1}$$

where WF is the water flux (L/m²/h), V is the collected permeate water volume (L), A is the effective area of the membrane (m², 28.7 cm²), and t is the permeation time (h). The WF characteristic of membranes was described according to the needed time for passing a specified volume of DI water through the membrane.

Salt rejection experiment was testing using 500 ppm NaCl and $MgSO_4$ aqueous solution as feed solutions. The concentrations of salt solution in feed and permeate were measured using the conductivity meter (Shanghai). The solute rejection was defined based on the following formula [45]:

$$R = \left(\frac{C_1 - C_2}{C_1}\right) \times 100\% \tag{2}$$

where C_1 and C_2 are the concentration of salt in feed and permeate, respectively. During the salt rejection test, the feed solutions were electrically stirred at a cell to reducing the negative effects of the concentration polarization phenomenon [6].

2.5. Water content

The water content was conducted to evaluate the water adsorption of the membrane [44]. All pieces of membranes were stored in DI water for 24 h and weighed after wiping water on the membrane surface. Later, the wet membranes were dried in a vacuum oven at 70°C for 4 h and weighed again. To minimize the experimental errors, the measurements were carried out 3 times for each sample, and then the mean value calculated using Eq. (3) was reported. The equation is listed as follows:

$$U = \left(\frac{W_w - W_d}{W_w}\right) \times 100\% \tag{3}$$

where W_w and W_d are the weight of wet membranes and dry membranes, respectively.

2.6. Molecular weight cutoff

The molecular weight cutoff (MWCO) of membranes was plotted by measuring the rejection of the polyethylene glycol (PEG) solutions with different molecular weights. The analytical method of the PEG concentrations in the feed and permeated solutions was UV spectrophotometry. The rejection of the protein (R) was calculated by the following equation:

$$R = 1 - \left(\frac{C_p}{C_f} \right) \times 100\% \quad (4)$$

where C_p and C_f are the permeate concentration and the feed concentration, respectively.

The membrane pore radius was measured on the basis of the PEG molecular weight and calculated as follows [46,47]:

$$y = -5 \times 10^{-8} x^2 + 5 \times 10^{-4} x + 0.3319 \quad (5)$$

where y is the pore radius (nm) and x is the molecular weight of PEG (g/mol).

2.7. Anti-fouling testing

The protein adsorption experiments were carried out with 500 ppm BSA solutions (pH 7.0). Before recording datum, membranes need to be preloaded with DI water under 0.15 MPa until reaching a steady flux (about 20 min). Afterwards the BSA solution was replaced, and the flux was measured once every 10 min continuously for 120 min. The membrane was washed with DI water for 30 min, and then measured the pure flux of the cleaned membrane was again. The flux recovery ratio (FRR) was calculated by the following equation:

$$\mathrm{FRR} = \frac{\mathrm{WF}_1}{\mathrm{WF}_0} \times 100\% \quad (6)$$

where WF_0 and WF_1 are the water fluxes of the initial and last time after washing for 30 min with DI water, respectively. The obtained flux datum was used to analyze the BSA fouling behavior of the membranes.

3. Results and discussion

3.1. BET of inorganic mesoporous silica (M-Si) and the membranes

The adsorption-desorption isotherms of liquid nitrogen for the inorganic M-Si particles are displayed in Fig. 2. All measured structural characteristics are listed in Table 1. The sample exhibited type IV isotherms with a typical H3 hysteresis loop according to IUPAC classification (which is associated with capillary condensation inside the pores), indicating that this sample belonged to the mesoporous family. The inorganic material showed a one-step capillary condensation, which demonstrated uniform mesopores. Additionally, from the BJH pore size distribution curves (Fig. 2a), the sample presented two sharp pore diameters of 3–4 nm and 5–6 nm. The pore structure of the sample is concentrated and uniform. This is mainly due to the fact that P123 is a triblock copolymer composed of PEO and PPO. The structure of the template affects the pore size distribution of mesoporous silicon directly. The silica sample exhibited large BET-specific surface areas (435.014 m^2/g). The BJH pore volume and average pore size were 0.771 cm^3/g and 5.689 nm, respectively. P123 was dissolved in ethanol solution in which the hydrophobic end polymerized to form micelles and the hydrophilic end was exposed in the solution to form a tubular stable micelle structure. Due to electrostatic interaction, TEOS binds to the hydrophilic

Table 1
Properties of the obtained mesoporous silica composite

Sample	M-Si
S_{BET} (m^2/g)	435.014
V_p (cm^3/g)	0.771
D_p (nm)	5.689

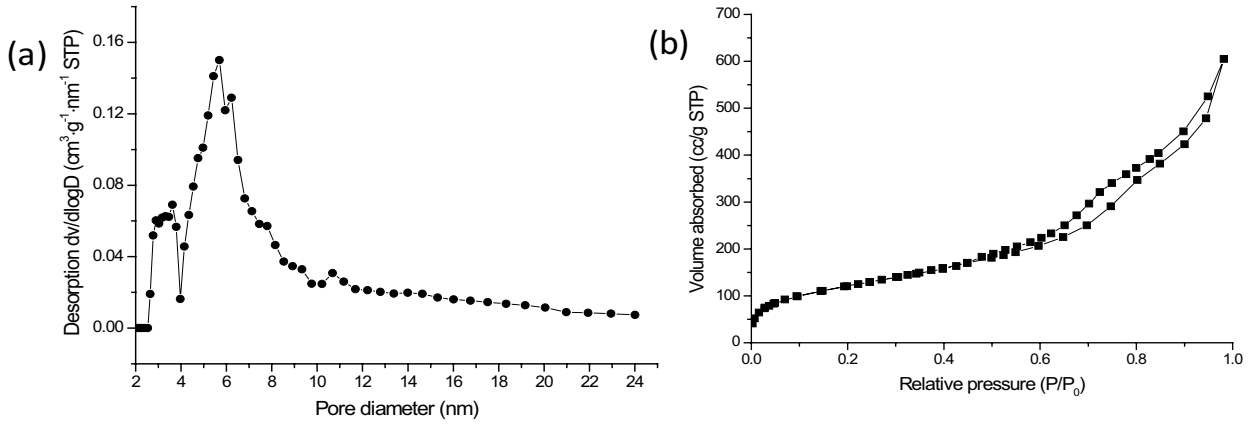

Fig. 2. Nitrogen adsorption–desorption isotherms of inorganic M-Si.

end of surfactant P123 after entering the solution. Then TEOS forms mesoporous silica particles due to hydrolysis in the acidic environment [48]. These results emphasize the successful synthesis of the M-Si materials.

In this paper, the pore size of the membrane was analyzed by BET. As shown in Fig. 3, the N_2 adsorption–desorption isotherm was compared with the pure and 0.2 wt.% blend membranes. When the partial pressure of P/P_0 is less than 0.2, the main adsorption style is single layer adsorption. At the same time when the N_2 partial pressure of P/P_0 is greater than 0.2, adsorption–desorption hysteresis loop appears because of the capillary condensation. According to the IUPAC classification, the N_2 adsorption–desorption isotherm curves of the films were II type and H3 type hysteresis loops, which indicated that the 2–50 nm mesoporous structure existed on the surface of the membrane. Fig. 3 shows that the blend film which was doped by 0.2 wt.% mesoporous silica has greater adsorption capacity and wider adsorption branch, this is due to the addition of mesoporous silica which increased the number of mesoporous structures on the surface of the blend film. The pore structure makes the desorption process more slowly and the desorption branch wider.

According to the principle of N_2 adsorption–desorption, the surface pore structure parameters of different blend films were obtained which are shown in Table 2. From Table 2, the specific surface area of the blend films is greatly improved because of adding of mesoporous silica when the doping amount reaches 1.0 wt.%, the specific surface area of the membrane is 14.487 m^2/g but the pore volume increased not obviously. The pore size of the blend film was reduced by an order of magnitude due to the doping of the mesoporous silica and the variation of the doping content had little effect on the pore size. The pure PES membrane consists of a support layer with long channels and a separation layer for screening. The macroporous support layer disappears and indeed a spongy structure forms because of the doping of mesoporous silicon which changes the structure of the film obviously. This is due to the formation of cross-linking structure between mesoporous silica precursor particles and polymers in the sol–gel process which blocks the formation of pores [49].

3.2. TEM and SXRD of the inorganic mesoporous silica (M-Si)

The TEM images (Fig. 4a) of mesoporous silica showed a highly ordered degree of periodicity; this further confirmed the 2-D hexagonal arrangement of pores with uniform sizes and well-aligned channels. Small-angle X-ray diffraction patterns for inorganic materials are shown in Fig. 4b. The inorganic mesoporous silica displayed three well-resolved diffraction peaks that can be indexed to (100), (110), and (200) reflections in low 2θ range at 0.90°, 1.48° and 1.66°, respectively. These peaks were indexed according to hexagonal p6mm symmetry, indicating a well-ordered mesostructure of the inorganic materials. This result was consistent with the previous studies [50,51]. The results show that the mesoporous structure of the material is uniform and has good long-range ordering, which corresponds well to the SXRD and N_2 adsorption-desorption analysis results.

3.3. Surface and cross-sectional morphologies of the membranes

The structure and morphology of the membranes before and after mingling were analyzed on the basis of SEM images. The membrane morphology exhibited the typical asymmetric structure, consisting of a skin layer as a selective layer and a supporting layer with a thick long-finger-like structure, just like the pure PES membrane showed (Fig. 5a). With the addition of M-Si, the supporting layer in blend membranes turned from a thick long-finger-like

Table 2
Properties of the blending membranes with different mesoporous silicon dosage

	Pore size (nm)	Surface area (m^2/g)	Pore volume (cm^3/g)
0%	47.34	5.438	0.06436
0.1%	2.744	7.045	0.05779
0.2%	2.146	9.622	0.066
0.5%	2.920	10.421	0.07607
1.0%	1.999	14.487	0.07238

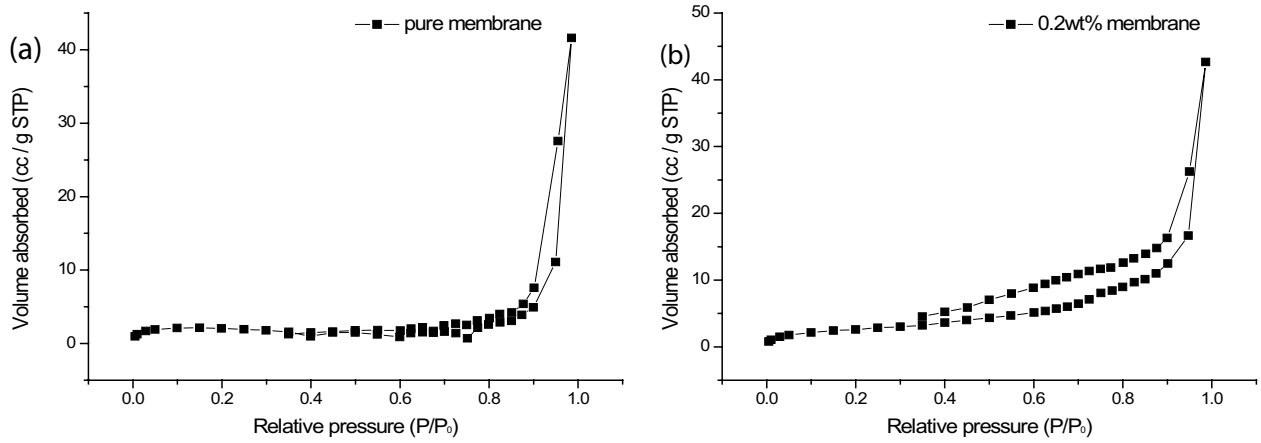

Fig. 3. Nitrogen adsorption–desorption isotherms of pure and 0.2 wt.% membranes.

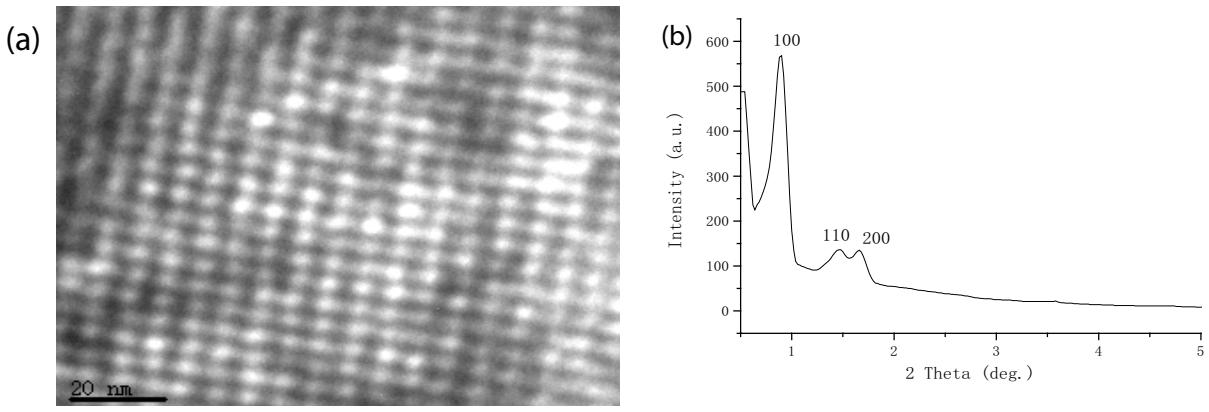

Fig. 4. TEM and small-angle X-ray diffractogram of the inorganic materials.

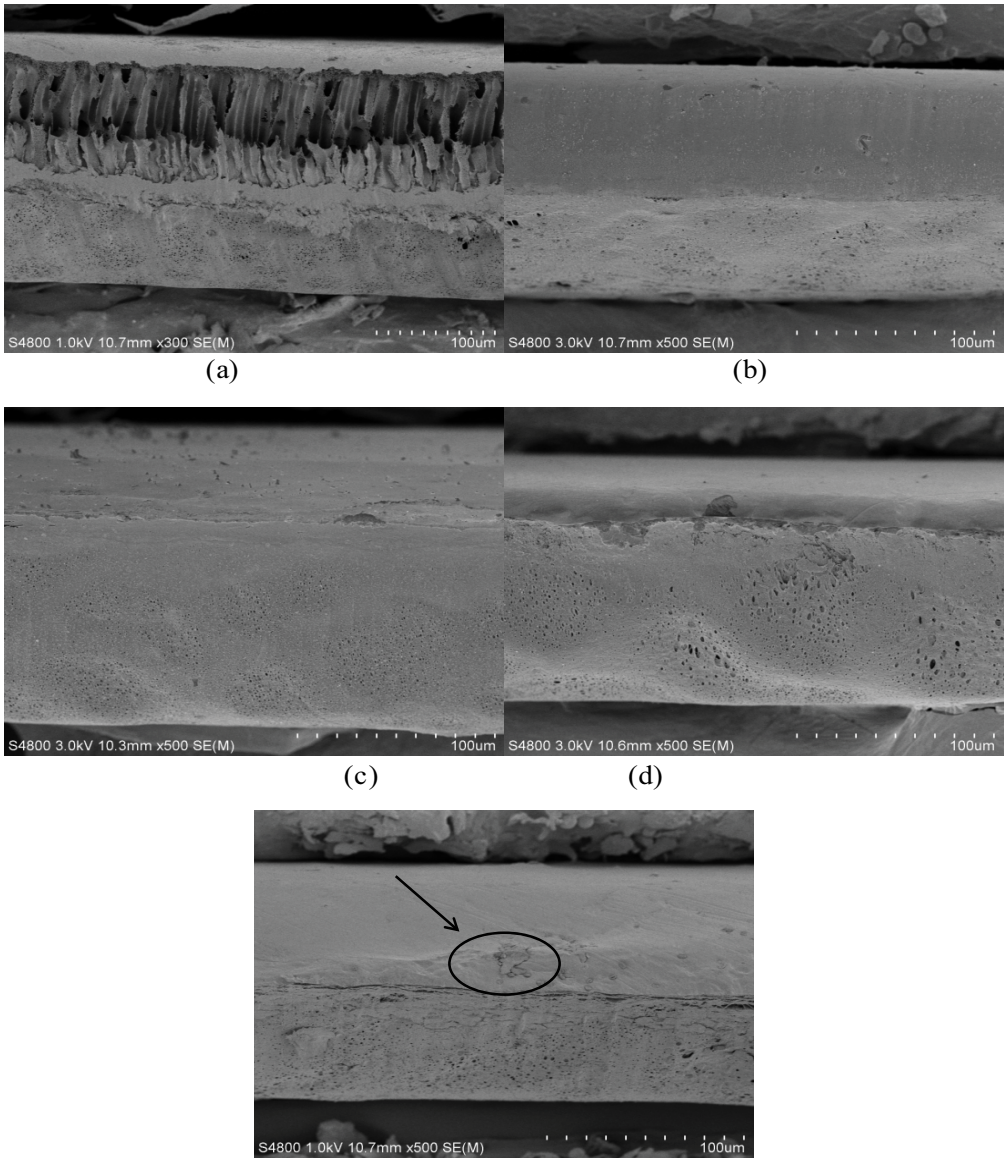

Fig. 5. Cross-sectional SEM images (scale bar: 100 μm) of the PES membranes with different loading of M-Si (0, 0.1, 0.2, 0.5 and 1.0 wt.%).

structure to a close sponge-like structure, which could be caused by the cross-linked structure between M-Si particles and polymeric chains after the sol–gel process resulting in a blocking effect for the formation of the finger-like cavities [52]. Fig. 5c (0.2 wt.% loadings) shows a typical transition from asymmetric structure to close sponge-like symmetrical structure, while in Fig. 5e (1.0 wt.% loading) nucleation nanoparticles and agglomeration phenomenon can be observed. The reason may be that under a low proportion of M-Si, the M-Si (pore diameter of 5.689 nm) was penetrated by polymer chains to form a homogenous casting solution [44]. However, overfull addition can cause inorganic nanoparticles forming agglomeration of large particles which decrease the homogeneity and viscosity. This is also consistent with the average pore size distribution of the PES membranes with different loading of M-Si.

Fig. 6 shows that the addition of M-Si can change the skin layer surface morphology compared with the pure PES membrane (a). The outer surface of blend membranes contented of 0.1 (b), 0.2 (c) and 0.5 (d) wt.% M-Si has some holes. This could be interpreted as the existence of the hydrophilic M-Si which has a higher affinity to water relative to PES increasing the penetration velocity of water in the surface of the membrane and the solvent diffusion velocity from the membrane to water [6]. Moreover, the smooth surface SEM image of the blend membrane with 1.0 wt.% (e) M-Si loading may be explained by the hindrance effect due to the agglomeration and formation of nanoparticles large clusters stunting the exchange between water and solvent into the nascent membrane. Fig. 6f (the blend membrane with 0.2 wt.% M-Si loading) shows that many white punctiform objects exist in the surface of the membrane indicated

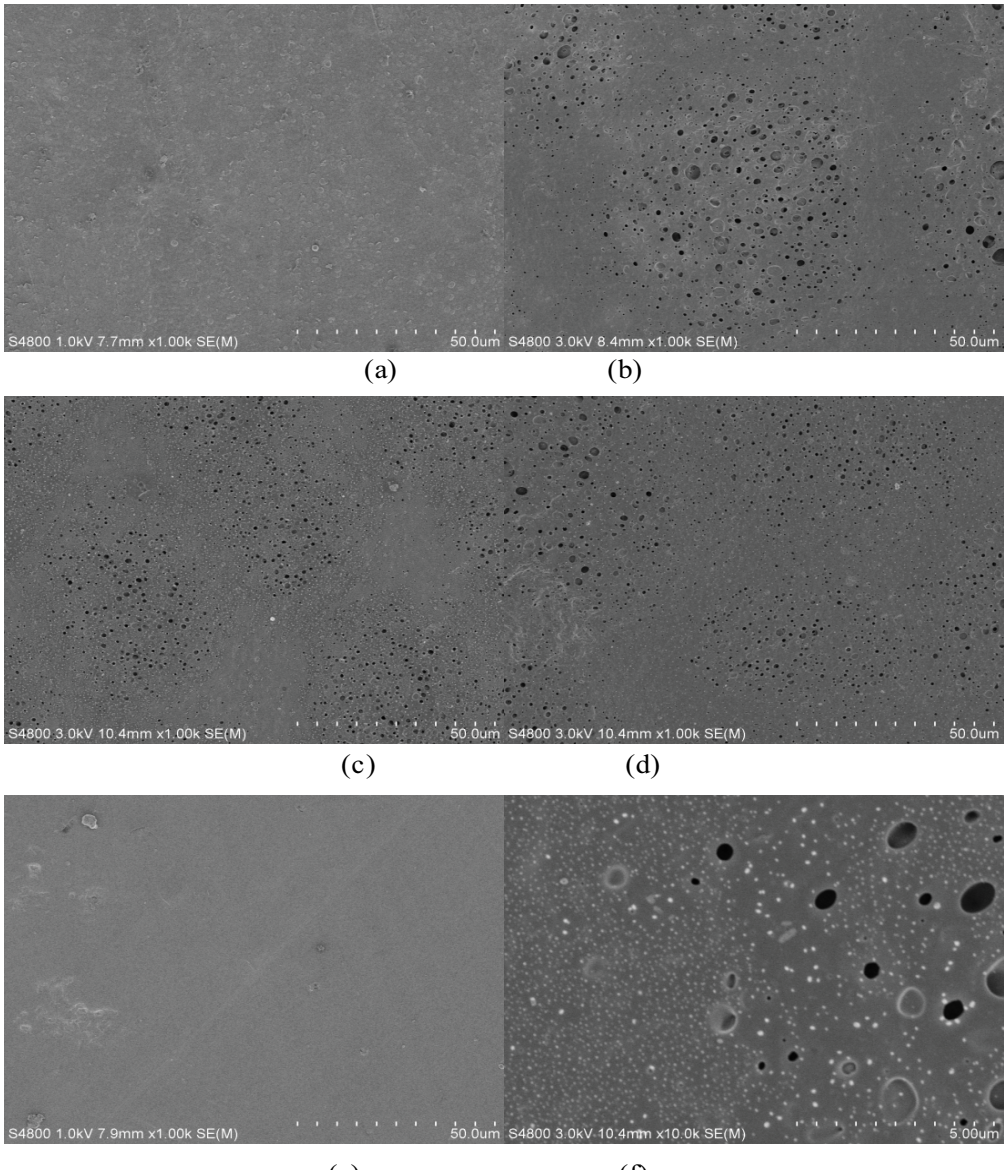

Fig. 6. Skin layer of outer surface morphologies (scale bar: 50 μm) of the membranes blended with 0 (a), 0.1 (b), 0.2 (c), 0.5 (d), 1.0 (e) wt.% M-Si, and surface SEM image of 0.2 wt.% blend membrane (scale bar: 5 μm) (f).

the presence of M-Si nanoparticles. Compared with the results of BET, it can be concluded that the increase of specific surface area of doped membrane is due to the formation of holes on the surface of films.

3.4. Viscosity analysis of the casting membranes liquid

The viscosity of casting membranes liquid can affect the exchange rate of solvent and non-solvent. In the blend membrane preparation process, we change the mass ratio of calcined mesoporous silica precursor and the casting membranes liquid with the same membrane sol conditions.

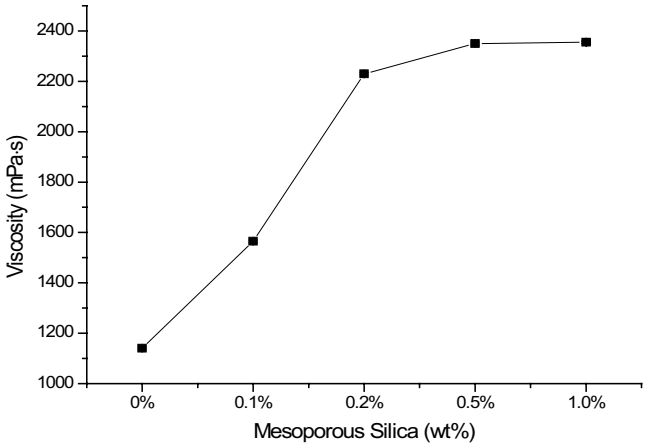

Fig. 7. The influence of different dope blending membranes in viscosity.

At last, we prepared a series of organic and inorganic membranes with different doping amount which are shown in Fig. 7. As can be seen from the figure, the doping of inorganic mesoporous silicon precursor can significantly improve the viscosity of the casting film and the viscosity is greater as the doping amount becomes higher. Because of the high-affinity material the inorganic mesoporous silica precursor is, the crosslinking structure can be formed between polymer and mesoporous silica precursor particles. So this can enhance the interaction among molecules in the casting membranes liquid and the viscosity shows increasing. However, when the doping amount is greater than 0.5 wt.%, the viscosity does not continue to increase which is due to the sediment of the mesoporous silicon precursors. Compared with results from SEM (Fig. 5), overfull addition can cause inorganic nanoparticles forming agglomeration of large particles which inhibits the increase of membrane viscosity.

3.5. XPS analysis of the membranes

In order to investigate the composition of the material and the valence state of the products, the XPS of the blend films with different contents was analyzed and the results are shown in Fig. 8 and Table 3. From Fig. 8a and Table 3, the pure film and the blend films all have sulfur, carbon, nitrogen, oxygen, combined with the electronic absorption peak of 167.17, 282.17, 399.17 and 531.17 eV respectively belong to S2p, C1s, N1s and O1s. In addition, the absorption peak of Si2p in the blend film was also found at 101.17 eV which proved the existence of silicon in the blend film.

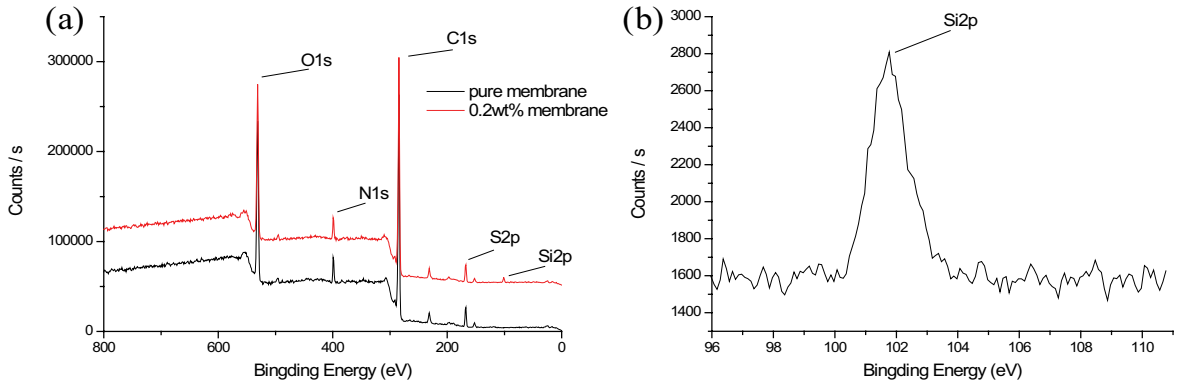

Fig. 8. (a) XPS spectra of pure and 0.2 wt.% membranes and (b) Si2p spectra of 0.2 wt.% membranes.

Table 3
Binging energies (BE) of core electrons and elements type of blending NF membranes with different mesoporous silicon dosage

Samples	O1s		N1s		C1s		S2p		Si2p	
	BE (eV)	%	BE (eV)	%	BE (eV)	%	BE (eV)	%	BE (eV)	%
0%	531.17	22.01	399.17	5.22	282.17	69.78	167.17	2.99		0
0.1%	531.17	23.57	399.17	3.5	282.1	66.88	168.17	5.41	101.17	0.64
0.2%	531.17	20.98	399.17	3.26	282.1	69.31	167.17	5.52	101.17	0.93
0.5%	531.17	21.37	399.17	4.96	282.1	69.08	167.17	3.05	101.17	1.53
1.0%	531.17	22.27	399.17	5.71	282.1	67.26	167.17	3.33	101.17	1.41

In Table 3, there is a linear relationship among the silicon content when the doping amount is less than 0.2 wt.%, but when the doping amount is higher than 0.2 wt.% the silicon content has been increased without linear proportion. At the same time, there is a decrease of silicon content when the doping amount reaches 1.0 wt.%, due to the fact that when the doping amount of the mesoporous silicon precursor is too high, the mesoporous silica precursor particles formed the aggregate to precipitate at the bottom in the casting membranes liquid.

In photoelectron spectroscopy, silicon atoms are characteristic absorption peaks in the vicinity of 99.3 eV and the absorption peak of tetravalent silicon is in the vicinity of 103.3 eV. From Fig. 8b a strong absorption peak near 101.77 eV appeared because of adding mesoporous silica precursor in blend films and no characteristic absorption peak at 99.3 eV which means the material is tetravalent forms rather than the atomic state on the surface of blend membrane. The synthesis process of mesoporous silica is the formation of hydrolysis of silica and then self-assembly with the template. So the tetrahedral structure on silicon has a certain spatial orientation as the center of the formation of Si–O.

3.6. SCA analysis of the membranes

The static contact angle is an important index to measure the hydrophilicity of the membrane and is also is the main index to evaluate the wettability of the solid surface. As shown in Fig. 9, the static contact angle of blend films with different content was lower than 90° indicating that the membranes are all hydrophilic. The static contact angle of doped mesoporous silica membranes decreased by nearly 10° compared with the pure membrane (79.4°). Because the mesoporous silica contains a large number of hydroxyl (–OH) hydrophilic groups, it enhanced appetency between membrane surface and hydrone which indicates that the addition of mesoporous silica can enhance the hydrophilicity of the membrane surface and is favorable for transmission of water. However, the static contact angle of the blend films with different doping amount was not significant (about 67°).

3.7. Zeta potential analysis of the membranes

Nanofiltration membrane can separate charged substances from water by the surface charge according to the Donnan exclusion effect. The separation effect of charged materials was directly affected by the surface charge density. The zeta potential values of the blend films with different amount of mesoporous silicon are shown in Fig. 10. As we have seen, the membrane surface is an amphoteric surface and the zeta potential value decreases with the increase of pH values. The isoelectric point of blend films was between 3.1–3.6 and all the membrane surface is positively charged when pH is less than 3.1. At the same time, the membrane surface was negatively charged when the pH is greater than 3.6. The pH value of general surface water is 6.5–8.5 and in this interval, the electronegativity of blend membranes increased about 18mV compared with the pure membrane in addition to 1.0 wt.% blend film. This is caused by the mesoporous silica doped on the membrane surface with hydroxyl groups, which enhance the negative potential energy of the membrane surface. However, the electronegativity of blend film with the maximum amount of doping material did not increase, mainly due to the aggregation of inorganic mesoporous silica made the content of the silicon in the mesoporous membrane, not uniform. The doping of the mesoporous silica did not significantly change the isoelectric point of the pure membranes.

3.8. Effect of mesoporous silica (M-Si) dosage on membrane permeability and salt rejection

The effect of M-Si dosage on permeability (WF) and salt (NaCl and $MgSO_4$) rejection are shown in Figs. 11 and 12, respectively, which shows that the addition of M-Si can reduce the WF obviously. Moreover, a membrane with the dosage of 0.2 wt.% M-Si achieves its minimum (10.45 L/m^2 h) and decreases by 62.12% compared to the pure membrane (27.60 L/m^2 h). This is mainly due to the structural and morphological changes of the membrane structure related to the addition of M-Si. Comparison of SEM images between the pure membrane and blend membranes showed that thick long-finger-like structure disappeared and was even well-distributed. It seems that the higher uniformity of

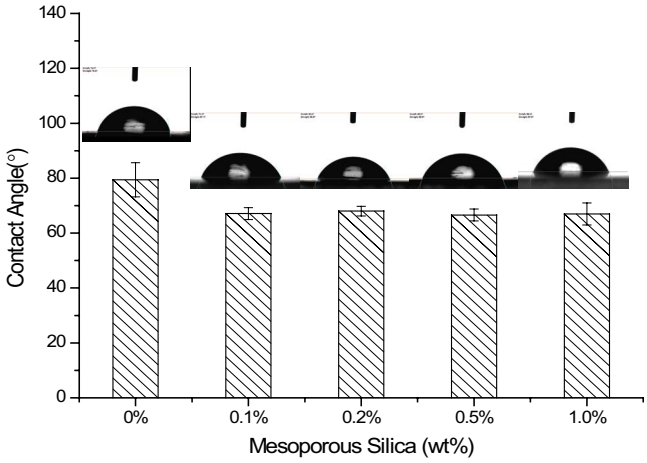

Fig. 9. Contact angles of blending NF membranes with different mesoporous silicon precursors dosage.

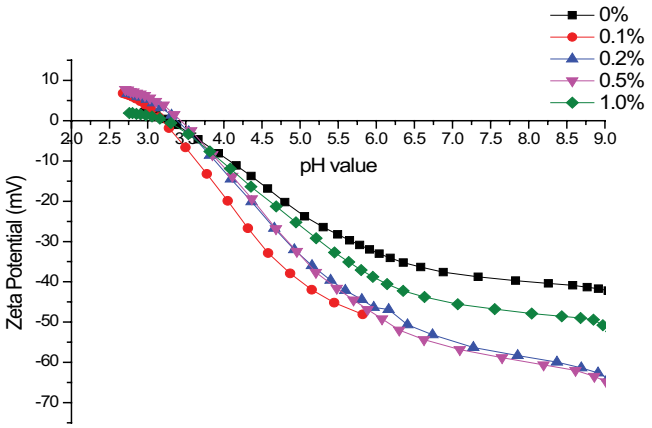

Fig. 10. Zeta potential vs. pH curves of blending NF membranes with different mesoporous silicon precursor dosage.

the membrane makes WF lower. When the doping of M-Si was more than 0.2 wt.%, the lower homogeneity of membranes and the larger dosage of hydrophilic M-Si particles resulted in the increase of WF [53].

The separation mechanism in NF membrane is affected in many aspects such as sieving, Donnan exclusion effect and differences in diffusivity and solubility of solute [54]. As shown in Fig. 12, the rejection of NaCl and $MgSO_4$ shows different behaviors with the increase of M-Si dosage. For NaCl solution, salt rejection is no fundamental change and the maximum (9.53%) is only 8.58% higher than the rejection of pure membrane (0.94%), which can be explained that the high diffusion coefficient for NaCl (1.61×10^{-9} m^2/s) [55] makes it have no change in the course of this experiment. While for $MgSO_4$ solution, the addition of M-Si increases the rejection remarkably. The increase of M-Si dosage from 0 to 1.0 wt.% is associated with the increase of rejection from 3.74% to 63.60%. This is possible that the compact change of supporting layer (SEM images) improves the sieving effect and magnifies the charge density of the membrane surface, resulting in the increase of $MgSO_4$ rejection. It seems that the rejection of salts in this study is effected by the combination of screening, Donnan exclusion effect and differences in diffusivity and solubility.

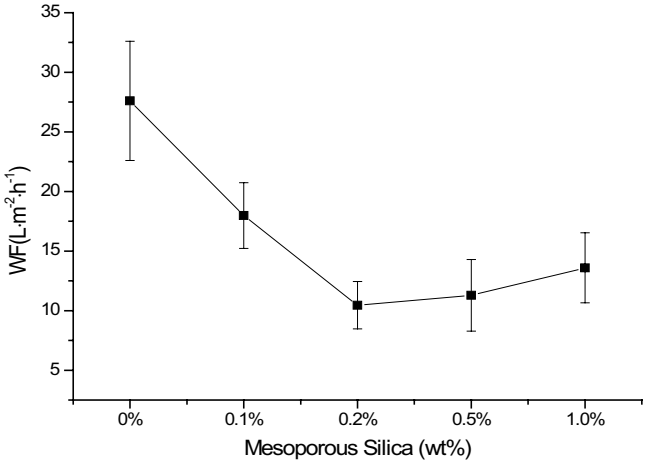

Fig. 11. Effect of M-Si dosage (wt.%) on the membrane water flux.

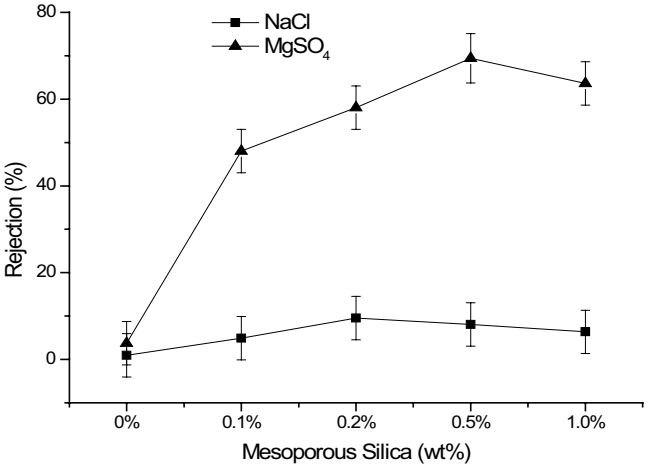

Fig. 12. Effect of M-Si dosage (wt.%) on NaCl and $MgSO_4$ rejection.

3.9. Water content of blend membranes with different M-Si dosage

The effect of M-Si concentration on membrane water content is shown in Fig. 13. According to Fig. 13, the water content of membranes reflecting the hydrophilicity and swelling can be changed by incorporating M-Si particles into substrate membrane [56,57]. Blend membrane with 0.1 wt.% dosage showed a little decrease compared to the pure film (71.67%), which could be explained that the shrink of membrane pore size and the structural changes due to the addition of M-Si reduced the pore volume. With the increase of M-Si concentration from 0.2 to 1.0 wt.%, the water content increased. This may be that in spite of large pores and macro-voids in the membrane structure disappeared, many dense compact holes formed, and increased the adsorption of water molecules because of the hydrophilic characteristic of M-Si particles. In other words, the water content of unit space for pore volume increased.

3.10. Molecular weight cutoff

Fig. 14 illustrates the rejection performance of the membranes blended with different dosages M-Si for 1,000 ppm PEG solutions with different molecular weights (400, 600, 1,000, and 2,000 Da). With the increase of MWCO value, the rejection increases. The best uniformity showed by a membrane with 0.2 wt.% dosage exhibits the highest rejection rate. As in previous studies, the smallest molecular weight which is rejected at 90% is taken as the MWCO of the membrane [58]. The membrane pore size is related to the MWCO of PEG and membrane pore radius measured by Eq. (5). It can be seen that the rejections of blend membranes (0.2, 0.5,1.0 wt.%) are greater than 90% for PEG solution (2,000 Da) and less than 90% for PEG solution (1,000 Da), which means that the pore radii of these membranes are between 0.78 and 2.13 nm.

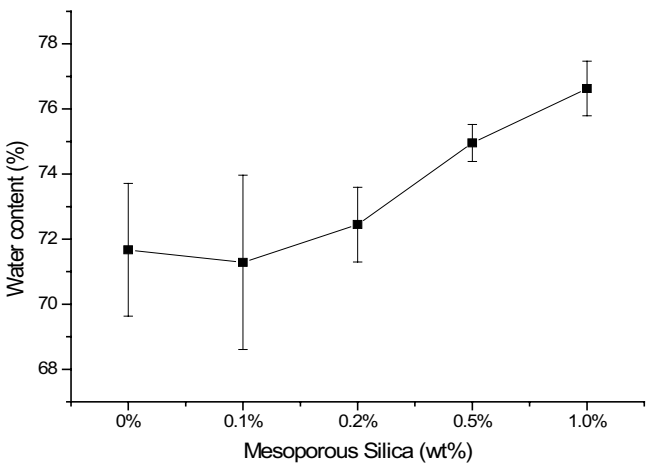

Fig. 13. The water content of blend membranes with different M-Si dosage.

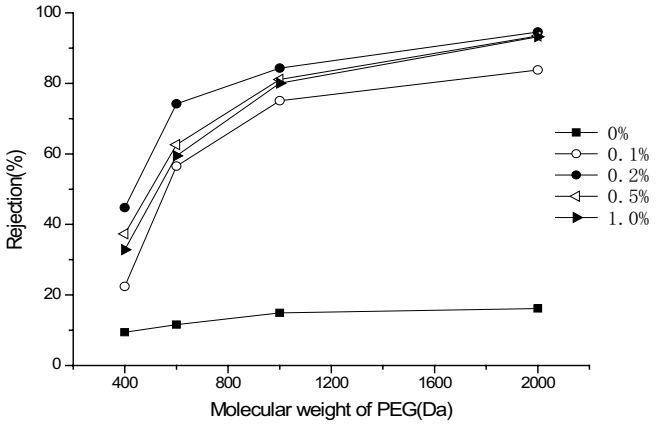

Fig. 14. Rejection of the PEG solutions with different molecular weights (400, 600, 1,000, and 2,000 Da) by blend membranes.

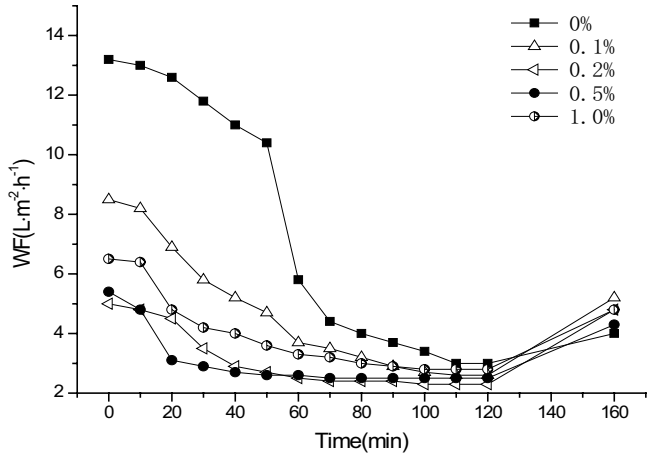

Fig. 15. Time-dependent WF during filtration of 500 ppm BSA solution at 0.15 MPa for membranes with different dosages of M-Si (0, 0.1, 0.2, 0.5, and 1.0 wt.%).

3.11. Anti-fouling performance of the membranes

Fig. 15 shows the time-dependent WF of pure water and BSA solution for the membranes. All membranes exhibit the drop of WF and reach the stable minimum (from 2.3 to 3 L/m^2 h). After washing for 30 min with DI water, all the WF is around 4.8 L/m^2 h. The WF of pure membrane drops more dramatically than blend membranes and reaches stabilizing spending much more time. This is maybe that the finger-like pores in the pure membrane make it easy to penetrate water molecules with protein. However, with the steady accumulation of protein in these pores which caused the blockage of the channel, the WF of the membrane drops abruptly. Furthermore, the relatively steady WF at last time is obtained because of the equilibrium accomplished between the deposition and sweeping of protein molecules on the membrane surface [59]. The rapid decline of WF is due to the poor anti-fouling ability of the membrane, which makes a large number of pollutants accumulate in the membrane channel. The stability of water flux data means that there are few pollutants in the membrane and the anti-fouling ability of the blend membrane is strong. In Fig. 16, flux recovery

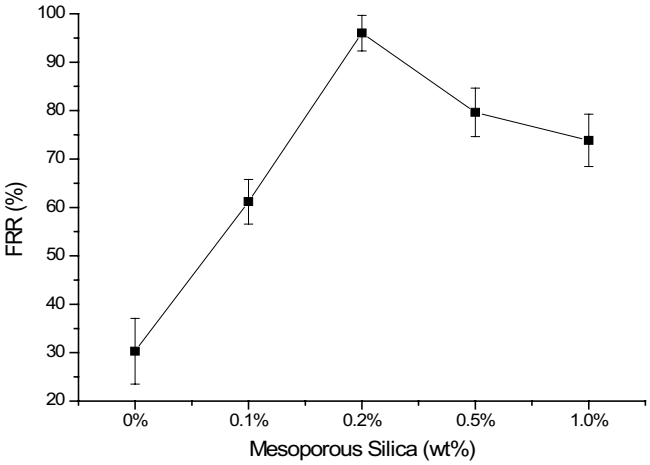

Fig. 16. Flux recovery ratio (FRR) for membranes with different dosages of M-Si (0, 0.1, 0.2, 0.5, and 1.0 wt.%).

ratio (FRR) for membranes shows that the addition of M-Si can improve the fouling resistance. FRR increases to the highest value to 96% as the M-Si loading increases to 0.2 wt.%, while FFR decreases to 73.85% with 1.0 wt.% M-Si content in the membrane. The reason is that the addition of hydrophilic M-Si improves the hydrophilcity of membrane surface for better anti-fouling properties [60], and they can be washed easily by simple water. Moreover, the change of blend membranes' internal structure due to the polymer chains as explained in section 3.2 made variation happened in pore size, resulting that protein molecules are hard to permeate and build up at the membrane surface. So we can see that there is no great change in WF with 0.2 wt.% M-Si content in membrane (Fig. 15). However, FRR is also related to the pore size of the membrane. The poor uniformity of the membrane makes it easy for protein molecules to gather on the surface of the membrane. Excessive doping will lead to the decrease of the uniformity of the membrane surface.

4. Conclusion

In this study, we developed a new method for synthesizing nanofiltration membrane blended with mesoporous silica (M-Si) using the phase inversion method. The microstructure, permeability, salt rejection, water content, MWCO and anti-fouling performance of modified membranes were altered because of the addition of M-Si. The main conclusions were listed as follows:

- The N_2 adsorption/desorption test, XPS analysis and SXRD indicated that well-ordered mesoporous silica could be doped in blend membrane synthesized by mingling with the precursor of M-Si without removal of the template and calcining in this condition after membrane forming.
- The SEM and MWCO results indicated that the cross-linked structure between M-Si particles and polymeric chains increased membrane uniformity, eliminated long-finger-like supporting layer and minified the pore size, resulting in a decrease of WF (10.45–17.98 L/m^2 h) compared to the pure membrane (27.60 L/m^2 h). The rejection of $MgSO_4$ has been improved due to the reinforced sieve

effect and intensified charge density. The results of viscosity, SCA and zeta potential test showed that the blend film modified mesoporous silica has a great improvement in the surface structure over the pure membrane.
- The water flux and salt rejection experiments manifested that adding M-Si particles in the membrane could decrease the water flux and improve $MgSO_4$ rejection because of the decrescent membrane pore size and reinforced charge density on the membrane surface.
- The water content and anti-fouling tests indicated that the addition of M-Si has improved membrane hydrophily by enhancing the water content of unit space for pore volume and anti-fouling property with a smaller change in WF and higher FRR. The best result was obtained for blend membrane with 0.2 wt.% loadings, showing the highest FRR (96%).
- NF membranes fabricated in this way can be conducted at 0.15 MPa, reducing the consumption of energy, which shows great potential for mass usage in micro-organic filtration and advanced water treatment.

Acknowledgments

Financial support for this research was provided by the Natural science research project of Jiangsu University (Grant No. 18KJB610014), the Scientific research project of Nanjing Xiaozhuang University (Grant No. 2018NXY51), Project 948: the water detection system trace volatile organic compounds (30155045912).

References

[1] L. Shao, X.Q. Cheng, Y. Liu, S. Quan, J. Ma, S.Z. Zhao, K.Y. Wang, Newly developed nanofiltration (NF) composite membranes by interfacial polymerization for Safranin O and Aniline blue removal, J. Membr. Sci., 430 (2013) 96–105.
[2] P.S. Zhong, N. Widjojo, T. Chung, M. Weber, C. Maletzko, Positively charged nanofiltration (NF) membranes via UV grafting on sulfonated polyphenylenesulfone (SPPSU) for effective removal of textile dyes from wastewater, J. Membr. Sci., 417 (2012) 52–60.
[3] L.Y. Jiang, Y. Wang, T. Chung, X.Y. Qiao, J. Lai, Polyimides membranes for pervaporation and biofuels separation, Prog. Polym. Sci., 34.11 (2009) 1135–1160.
[4] J.P. Chen, H. Mou, L.K. Wang, T. Matsuura, Y. Wei, Membrane Separation: Basics and Applications, Handbook of Environmental Engineering, Humana Press, 2011, pp. 271–332.
[5] L.M. Jin, S.L. Yu, W.X. Shi, X.S. Yi, N. Sun, Y.L. Ge, C. Ma, Synthesis of a novel composite nanofiltration membrane incorporated SiO_2 nanoparticles for oily wastewater desalination, Polymer, 53 (2012) 5295–5303.
[6] P. Mobarakabad, A.R. Moghadassi, S.M. Hosseini, Fabrication and characterization of poly(phenylene ether-ether sulfone) based nanofiltration membranes modified by titanium dioxide nanoparticles for water desalination, Desalination, 365 (2015) 227–233.
[7] A. Rahimpour, M. Jahanshahi, N. Mortazavian, S.S. Madaeni, Y. Mansourpanah, Preparation and characterization of asymmetric polyethersulfone and thin-film composite polyamide nanofiltration membranes for water softening, Appl. Surf. Sci., 256 (2010) 1657–1663.
[8] A. Abdullah, Al-Hajouri, S. Ahmed, Al-Amoudi, Long term experience in the operation of nanofiltration pretreatment unit for seawater desalination at SWCC SWRO plant, Desal. Water Treat., 51 (2013) 1861–1873.
[9] A.W. Mohammad, R. Othaman, N. Hilal, Modelling the effects of nanofiltration membrane properties on system cost assessment for desalination applications, Desalination, 168 (2014) 241–252.
[10] D. Wu, W. Wang, S. Chen, Z. Yang, G. Tian, S.A. Baig, Q. Mahmood, Advanced bamboo industry wastewater treatment through nanofiltration membrane technology, Desal. Water. Treat., 51 (2013) 3454–3462.
[11] H. Song, J. Shao, Y. He, J. Hou, W. Chao, Natural organic matter removal and flux decline with charged ultrafiltration and nanofiltration membranes, J. Membr. Sci., 376 (2011) 179–187.
[12] A. Caus, S. Vanderhaegen, L. Braeken, B. Van der Bruggen, Integrated nanofiltration cascades with low salt rejection for complete removal of pesticides in drinking water production, Desalination, 241 (2009) 111–117.
[13] S. Xia, B. Dong, Q. Zhang, B. Xu, N. Gao, C. Causseranda, Study of arsenic removal by nanofiltration and its application in China, Desalination, 204 (2007) 374–379.
[14] R.S. Harisha, K.M. Hosamani, R.S. Keri, S.K. Nataraj, T.M. Aminabhavi, Arsenic removal from drinking water using thin film composite nanofiltration membrane, Desalination, 252 (2010) 75–80.
[15] A. Favre-Réguillon, G. Lebuzit, D. Murat, J. Foos, C. Mansour, M. Draye, Selective removal of dissolved uranium in drinking water by nanofiltration, Water Res., 42 (2008) 1160–1166.
[16] B. Xu, D. Li, W. Li, S. Xia, Y. Lin, C. Hu, C. Zhang, N. Gao, Measurements of dissolved organic nitrogen (DON) in water samples with nanofiltration pretreatment, Water Res., 44 (2010) 5376–5384.
[17] G.E. Chen, Y.J. Liu, Z.L. Xu, D. Hu, H.H. Huang, L. Sun, Preparation and characterization of a composite nanofiltration membrane from cyclen and trimesoyl chloride prepared by interfacial polymerization, J. Appl. Polym. Sci., 132 (2015) 478–496.
[18] J. Liu, Z. Xu, X. Li, Y. Zhang, Y. Zhou, Z. Wang, X. Wang, An improved process to prepare high separation performance PA/PVDF hollow fiber composite nanofiltration membranes, Sep. Purif. Technol., 58 (2007) 53–60.
[19] J. Zhu, Q. Zhang, S. Li, S. Zhang, Fabrication of thin film composite nanofiltration membranes by coating water soluble disulfonated poly(arylene ether sulfone) and in situ crosslinking, Desalination, 387 (2016) 25–34.
[20] Y. Ji, Q. An, Q. Zhao, W. Sun, K. Lee, H. Chen, C. Gao, Novel composite nanofiltration membranes containing zwitterions with high permeate flux and improved anti-fouling performance, J. Membr. Sci., 390 (2012) 243–253.
[21] C. Feng, J. Xu, M. Li, Y. Tang, C. Gao, Studies on a novel nanofiltration membrane prepared by cross-linking of polyethyleneimine on polyacrylonitrile substrate, J. Membr. Sci., 451 (2014) 103–110.
[22] M. Safarpour, V. Vatanpour, A. Khataee, Preparation and characterization of graphene oxide/TiO_2 blended PES nanofiltration membrane with improved antifouling and separation performance, Desalination, 393 (2016) 65–78.
[23] J. Zhang, Q. Wang, Z. Wang, Modification of poly(vinylidene fluoride)/polyethersulfone blend membrane with polyvinyl alcohol for improving antifouling ability, J. Membr. Sci., 466 (2014) 293–301.
[24] K. Ekambaram, M. Doraisamy, Study on the fabrication, characterization and performance of PVDF/calcium stearate composite nanofiltration membranes, Desalination, 385 (2016) 24–38.
[25] H. Mahdavi, F. Ardeshiri, An efficient nanofiltration membrane based on blending of polyethersulfone with modified (styrene/maleic anhydride) copolymer, J. Iran. Chem. Soc., 13 (2016) 873–880.
[26] G.S. Lai, W.J. Lau, P.S. Goh, A.F. Ismail, N. Yusof, Y.H. Tan, Graphene oxide incorporated thin film nanocomposite nanofiltration membrane for enhanced salt removal performance, Desalination, 387 (2016) 14–24.
[27] H. Adib, S. Hassanajili, M.R. Sheikhi-Kouhsar, A. Salahi, T. Mohammadi, Experimental and computational investigation of polyacrylonitrile ultrafiltration membrane for industrial oily wastewater treatment, Korean J. Chem. Eng., 32 (2015) 159–167.
[28] A. Bottino, G. Capannelli, V. D'Asti, P. Piaggio, Preparation and properties of novel organic–inorganic porous membranes, Sep. Purif. Technol., 22 (2011) 269–275.

[29] T. Chung, M.L. Chng, K.P. Pramoda, Y. Xiao, PAMAM dendrimer-induced cross-linking modification of polyimide membranes, Langmuir, 20 (2004) 2966–2969.
[30] R. Pang, X. Li, J. Li, Z. Lu, X. Sun, L. Wang, Preparation and characterization of ZrO_2/PES hybrid ultrafiltration membrane with uniform ZrO_2 nanoparticles, Desalination, 332 (2014) 60–66.
[31] L. Yan, Y.S. Li, C.B. Xiang, S. Xianda, Effect of nano-sized Al_2O_3-particle addition on PVDF ultrafiltration membrane performance, J. Membr. Sci., 276 (2006) 162–167.
[32] N. Maximous, G. Nakhla, K. Wong, W. Wan, Optimization of Al_2O_3/PES membranes for wastewater filtration, Sep. Purif. Technol., 73 (2010) 294–301.
[33] G. Arthanareeswaran, T.S. Devi, M. Raajenthiren, Effect of silica particles on cellulose acetate blend ultrafiltration membranes: Part I, Sep. Purif. Technol., 64 (2008) 38–47.
[34] J. Shen, H. Ruan, L. Wu, C. Gao, Preparation and characterization of PES–SiO_2 organic–inorganic composite ultrafiltration membrane for raw water pretreatment, Chem. Eng. J., 168 (2011) 1272–1278.
[35] Z. Yi, L. Zhu, Y. Xu, Y. Zhao, X. Ma, B. Zhu, Polysulfone-based amphiphilic polymer for hydrophilicity and fouling-resistant modification of polyethersulfone membranes, J. Membr. Sci., 365 (2010) 25–33.
[36] Z. Yang, Z. Niu, X. Cao, Z. Yang, Y. Lu, Z. Hu, C.C. Han, Template synthesis of uniform 1D mesostructured silica materials and their arrays in anodic alumina membranes, Angew. Chem. Int. Ed., 42 (2003) 4201–4203.
[37] W. Zhu, Y. Han, L. An, Silver nanoparticles synthesized from mesoporous Ag/SBA-15 composites, Microporous Mesoporous Mater., 84 (2005) 69–74.
[38] Y. Chen, A. Yamaguchi, T. Atou, K. Morita, N. Teramae, Template synthesis of arrays of one-dimensional gold nanowires standing on a carbon film, Chem. Lett., 35 (2006) 1352–1353.
[39] K.J. Lee, S.H. Min, J. Jang, Vapor-phase synthesis of mesostructured silica nanofibers inside porous alumina membranes, Small, 4 (2008) 1945–1949.
[40] B. Platschek, R. Köhn, M. Döblinger, T. Bein, In situ GISAXS study of the formation of mesostructured phases within the pores of anodic alumina membranes, Langmuir, 24 (2008) 5018–5023.
[41] A. Yamaguchi, H. Kaneda, W. Fu, N. Teramae, Structural control of surfactant-templated mesoporous silica formed inside columnar alumina pores, Adv. Mater., 20 (2008) 1034–1037.
[42] D. Zhao, J. Sun, Q. Li, Morphological control of highly ordered mesoporous silica SBA-15, Chem. Mater., 12 (2000) 275–279.
[43] M.V. Lombardo, M. Videla, A. Calvo, F.G. Requejo, G.J.A.A. Soler-Illia. Aminopropyl-modified mesoporous silica SBA-15 as recovery agents of Cu(II)-sulfate solutions: adsorption efficiency, functional stability and reusability aspects, J. Hazard. Mater., 223–224 (2012) 53–62.
[44] J. Huang, K. Zhang, K. Wang, Z. Xie, B. Ladewig, H. Wang, Fabrication of polyethersulfone-mesoporous silica nanocomposite ultrafiltration membranes with antifouling properties, J. Membr. Sci., 423 (2012) 362–370.
[45] Y. Ma, F. Shi, J. Ma, M. Wu, J. Zhang, C. Gao, Effect of PEG additive on the morphology and performance of polysulfone ultrafiltration membranes, Desalination, 272 (2011) 51–58.
[46] M.D. Afonso, G. Hagmeyer, R. Gimbel, Streaming potential measurements to assess the variation of nanofiltration membranes surface charge with the concentration of salt solutions, Sep. Purif. Technol., 22 (2011) 529–541.
[47] A. Akbari, H. Solymani, S.M.M. Rostami, Preparation and characterization of a novel positively charged nanofiltration membrane based on polysulfone, J. Appl. Polym. Sci., 132 (2015) 235–246.
[48] C.H. Lee, T.S. Jeong, Y.K. Choi, B.H. Hyun, G.T. Oh, E.H. Kim, Anti-atherogenic effect of citrus flavonoids, naringin and naringenin, associated with hepatic ACAT and aortic VCAM-1 and MCP-1 in high cholesterol-fed rabbits, Biochem. Biophys. Res. Commun., 284 (2001) 681–688.
[49] L.Y. Yu, Z.L. Xu, H.M. Shen, H. Yang, Preparation and characterization of PVDF–SiO_2 composite hollow fiber UF membrane by sol–gel method, J. Membr. Sci., 337 (2009) 257–265.
[50] F. Rehman, A. Rahim, C. Airoldi, P.L. Volpe, Preparation and characterization of glycidyl methacrylate organo bridges grafted mesoporous silica SBA-15 as ibuprofen and mesalamine carrier for controlled release, Mater. Sci. Eng. C, 59 (2016) 970–979.
[51] A. Feliczak-Guzik, B. Jadach, H. Piotrowska, M. Murias, J. Lulek, I. Nowak, Synthesis and characterization of SBA-16 type mesoporous materials containing amine groups, Microporous Mesoporous Mater., 220 (2016) 231–238.
[52] L. Yu, Z. Xu, H. Shen, H. Yang, Reduction in threading dislocation densities in AlN epilayer by introducing a pulsed atomic-layer epitaxial buffer layer, J. Membr. Sci., 337 (2009) 257–265.
[53] A. Pk, A. Yi, B. Swha, C. Pls, B. Fba, Fabrication of novel polyethersulfone (PES) hybrid ultrafiltration membranes with superior permeability and antifouling properties using environmentally friendly sulfonated functionalized polydopamine nanofillers, Sep. Purif. Technol., 261 (2021) 362–370.
[54] J. Peeters, J.P. Boom, M. Mulder, H. Strathmann, Retention measurements of nanofiltration membranes with electrolyte solutions, J. Membr. Sci., 145 (1998) 199–209.
[55] I. Kim, K. Lee, T. Tak, Preparation and characterization of integrally skinned uncharged polyetherimide asymmetric nanofiltration membrane, J. Membr. Sci., 183 (2001) 235–247.
[56] S. Ansari, A.R. Moghadassi, S.M. Hosseini, Fabrication of novel poly(phenylene ether ether sulfone) based nanocomposite membrane modified by Fe_2NiO_4 nanoparticles and ethanol as organic modifier, Desalination, 357 (2015) 189–196.
[57] M. Sivakumar, D.R. Mohan, R. Rangarajan, Studies on cellulose acetate-polysulfone ultrafiltration membranes, J. Membr. Sci., 268 (2006) 208–219.
[58] K.J. Kim, A.G. Fane, R.B. Aim, M.G. Liu, G. Jonsson, I.C. Tessaro, A.P. Broek, D. Bargeman, A comparative study of techniques used for porous membrane characterization: pore characterization, J. Membr. Sci., 87 (1994) 35–46.
[59] M. Sun, Y. Su, C. Mu, Z. Jiang, Improved antifouling property of PES ultrafiltration membranes using additive of silica PVP nanocomposite, Ind. Eng. Chem. Res., 49 (2009) 790–796.
[60] J.H. Yi, F.Q. Zhao, H.X. Gao, Preparation, characterization, non-isothermal reaction kinetics, thermodynamic properties, and safety performances of high nitrogen compound: hydrazine 3-nitro-1,2,4-triazol-5-one complex, J. Membr. Sci., 153 (2008) 261–268.